

3D simulations of a magnetized Hall Effect thruster plume

IEPC-2019-460

*Presented at the 36th International Electric Propulsion Conference
University of Vienna, Austria
September 15-20, 2019*

Filippo Cichocki ^{*}, Adrián Domínguez-Vázquez [†], Mario Merino [‡], Pablo Fajardo [§] and Eduardo Ahedo [¶]
Equipo de propulsión espacial y plasmas (EP2), Universidad Carlos III de Madrid, Leganés, Spain

A three-dimensional hybrid PIC/fluid code is used to simulate a Hall Effect thruster plume, starting from a known injection profile at the annular exit section. The electron model features magnetized electrons and considers both anomalous transport and a polytropic closure for the electron temperature. Simulations with a varying anomalous transport coefficient show that it only affects importantly the predicted azimuthal current densities, if electron and heavy particles fluxes at the upstream boundary are kept fixed. The effects of a polytropic closure for the electron temperature are assessed by comparing the results with those of a companion 2D code that solves the electron energy equation. It is found that the polytropic characterization of the electron temperature induces important differences in the electric potential distribution downstream, except at the very beginning of the expansion. Moreover, a simulation featuring a lateral neutralizer position shows that the induced asymmetry is important for the electron and electric current density and streamlines, but negligible for the electric potential and heavy particle properties downstream, thus justifying the use of axisymmetric codes for Hall thrusters performance evaluation.

Nomenclature

Φ	= thermalized potential
ϕ	= electric potential
\mathbf{E}	= electric field vector
\mathbf{B}	= magnetic induction field vector
e	= elementary electron charge
m_e	= elementary electron mass
m_s	= elementary mass of the s^{th} heavy particle population
χ	= effective Hall parameter (effective)
h_e	= electron barotropy function
n_e	= electron number density
n_s	= number density of s^{th} heavy particle population
p_e	= electron pressure
T_e	= electron temperature

^{*}Assistant professor, Aerospace Engineering department, fcichock@ing.uc3m.es.

[†]PhD student, Aerospace Engineering department, addoming@ing.uc3m.es.

[‡]Associate professor, Aerospace Engineering department, mario.merino@uc3m.es

[§]Associate professor, Aerospace Engineering department, pablo.fajardo@uc3m.es

[¶]Professor, Aerospace Engineering department, eduardo.ahedo@uc3m.es

σ_e	= electron scalar conductivity
\mathcal{K}	= normalized conductivity tensor
ν_{es}	= electron momentum transfer frequency with the s^{th} heavy particle population
ν_e	= total electron momentum transfer collision frequency
Z_s	= charge number of the s^{th} heavy particle population
\mathbf{u}_e	= electron fluid velocity
\mathbf{u}_s	= fluid velocity of the s^{th} heavy particle population
\mathbf{g}_e	= electron flux vector
\mathbf{g}_s	= flux vector of the s^{th} heavy particle population
\mathbf{j}_i	= total ion current density vector
\mathbf{j}_e	= electron current density vector
\mathbf{j}_c	= collisional current density vector
\mathbf{r}_j	= individual position vector of the j^{th} macro-particle
\mathbf{v}_j	= individual velocity vector of the j^{th} macro-particle
Δt	= PIC time step for advancing macro-particles

I. Introduction

As the maturity of electric satellite platforms is rapidly increasing, the characterization of electric thrusters is becoming very demanded from the industry, especially to model the effects of their plasma plumes on the platform.^{1,2} These include spacecraft charging due to the impingement of core plume ions and charge-exchange ions (CEX) on the spacecraft, but also the consequent material contamination and sputtering, which are especially relevant for sensitive surfaces like the solar arrays, optical cameras and other on-board instruments.

Many existing codes solve simultaneously both the internal plasma discharge and the very-near plume of such thrusters,³⁻⁶ without focusing on the far-region plume expansion. One relevant class of such codes consists in a hybrid PIC-fluid model, in which ions are treated as macro-particles and electrons as a fluid. Inside the chamber, the ionization and energy sink reactions are dominant, and the electron fluid is far from being barotropic, meaning that the electron temperature is not a function of their density. Therefore, the electron pressure must be obtained by solving an energy balance equation, which is typically closed at the level of the heat flux vector. On the other hand, as ionization collisions quickly drop outside the discharge chamber, electron kinetic behaviour quickly becomes near-collisionless, and several plume experimental characterizations^{7,8} have reported a nearly polytropic one (a particular case of barotropy) at distances of around 50 cm from the thruster exit section. This assumption is made by a novel 3D hybrid PIC-fluid code, EP2PLUS,⁹⁻¹¹ whose electron fluid model additionally considers elastic collisions (with the heavy species), anomalous transport (through an equivalent transport coefficient⁶), and magnetization effects, which are especially relevant in the near plume of many plasma thrusters. This model was already presented at the Space Propulsion conference 2018,¹¹ where it was applied to a plasma plume expansion under a uniform geomagnetic field.

Being a hybrid code, EP2PLUS treats both ions and neutrals as macro-particles of a PIC sub-model, considering the effects of collisions such as single and double ionization events or charge-exchange (CEX) reactions between neutrals and singly-doubly charged ions.¹⁰ The electron model, on the other hand, solves for the electric potential and the other electron properties (e.g. temperature, density, and fluid velocity) by solving a non-linear Poisson equation (neglected in this work by assuming quasineutrality) and the system arising from the electric current continuity equation and the electron momentum balance equation. This latter equation includes the effects of both collisions with the heavy species and magnetization effects due to the local magnetic field.

In this paper, EP2PLUS is applied to the simulation of a magnetized Hall effect thruster (HET) plasma plume. The initial plasma profiles at the thruster exhaust section are obtained from the results of a companion 2D code, HYPHEN, also presented at this conference and described in Ref. 4. The major model simplification consists in assuming the above mentioned polytropic electron behavior rather than solving an electron energy balance equation. This assumption is clearly inadequate inside the discharge chamber, although it is not clear to what extent it affects the solution in the near-plume region. Therefore, the results obtained are compared with those of the 2D code to assess such effects. Moreover, while in the 2D code, the neutralizer

is located off-axis and is represented by an axisymmetric ring, the 3D code is run with two configurations: (i) a neutralizer on the axis, and (ii) a neutralizer located off-axis and hence non-symmetric. The effects of changing the position of the neutralizer and hence breaking the symmetry are evaluated to justify the implicit assumption of 2D axisymmetric codes that the neutralizer can be considered symmetric, without large impact on the electric potential distribution in the near-plume.

In the following, the hybrid PIC-fluid model and its particularities for this simulation scenario are briefly introduced in Sec. II, while the simulation setup is detailed in Sec. III A. Regarding the simulations, the nominal case results are presented in Sec. III B, while the effects of varying the anomalous transport coefficient and the neutralizer position are discussed in respectively Sec. III C and Sec. III D. Finally, the comparison with the 2D model results is presented in Sec. III E, and the conclusions are drawn in Sec. IV.

II. EP2PLUS hybrid model

A. The PIC model

The PIC model considered for the characterization of the heavy particles (neutrals and ions) is fully described in Ref. 10 and, in the following, we provide only a short summary. As in all PIC approaches, the particle distribution functions are discretized in the position-velocity phase-space with a given number of macro-particles, each representing W_j elementary particles and having position \mathbf{r}_j . Their bulk properties, like their number density, fluid velocity and temperature, are then obtained by weighting these macro-particles to the nodes of a structured PIC mesh,¹² here assumed to be Cartesian. For each time step Δt , the PIC sub-model performs operations such as:

1. moving the macro-particles according to Newton law, that is, for the j^{th} macro-particle:

$$\frac{d\mathbf{v}_j}{dt} = eZ_j [\mathbf{E}(\mathbf{r}_j) + \mathbf{v}_j \times \mathbf{B}(\mathbf{r}_j)], \quad (1)$$

where \mathbf{E} and \mathbf{B} are the electric and magnetic field at the macro-particle position, \mathbf{v}_j is the macro-particle velocity, and Z_j is the charge number of the macro-particle population (e.g. 1 for singly-charged ions, 2 for doubly-charged ions, and 0 for neutrals);

2. injecting new macro-particles into the simulation from the boundaries (see Fig. 1);
3. performing collisions between macro-particles (e.g. charge-exchange collisions, CEX), and generating/eliminating macro-particles due to sink/source collisional events (e.g. ionization);
4. weighting the macro-particles to the mesh nodes to obtain their fluid properties (used by the electron model);

Regarding the modeled collisions, these include different types of CEX and ionization collisions, as further mentioned in Sec. III A. Referring to Fig. 1, ions and neutrals are injected from the annular channel exit section, following the profiles obtained in the simulations of a companion paper,⁴ carried out with a 2D hybrid particle code, HYPHEN. Macro-particles are then simply lost when they cross the external boundaries of the simulation domain. If ions hit the front material walls of the thruster, they are recombined into neutrals, which are injected into the simulation domain diffusely, with a perfect thermal accommodation with the wall.¹⁰ Neutrals hitting such walls, on the other hand, are also diffusely reflected.

B. The magnetized electron model

The magnetized electron model takes as input the weighted properties of the PIC heavy species populations and computes self-consistently the electric potential ϕ and field $\mathbf{E} = -\nabla\phi$ required by the PIC sub-model, and other relevant electron properties, such as their density n_e , temperature T_e and current density \mathbf{j}_e . Although the EP2PLUS code is capable of solving a non-linear Poisson equation to obtain both the electric potential and the electron density,¹⁰ in the context of this study, quasineutrality has been assumed. Therefore, the electron density is directly retrieved from the PIC sub-model inputs as:

$$n_e = \sum_s Z_s n_s, \quad (2)$$

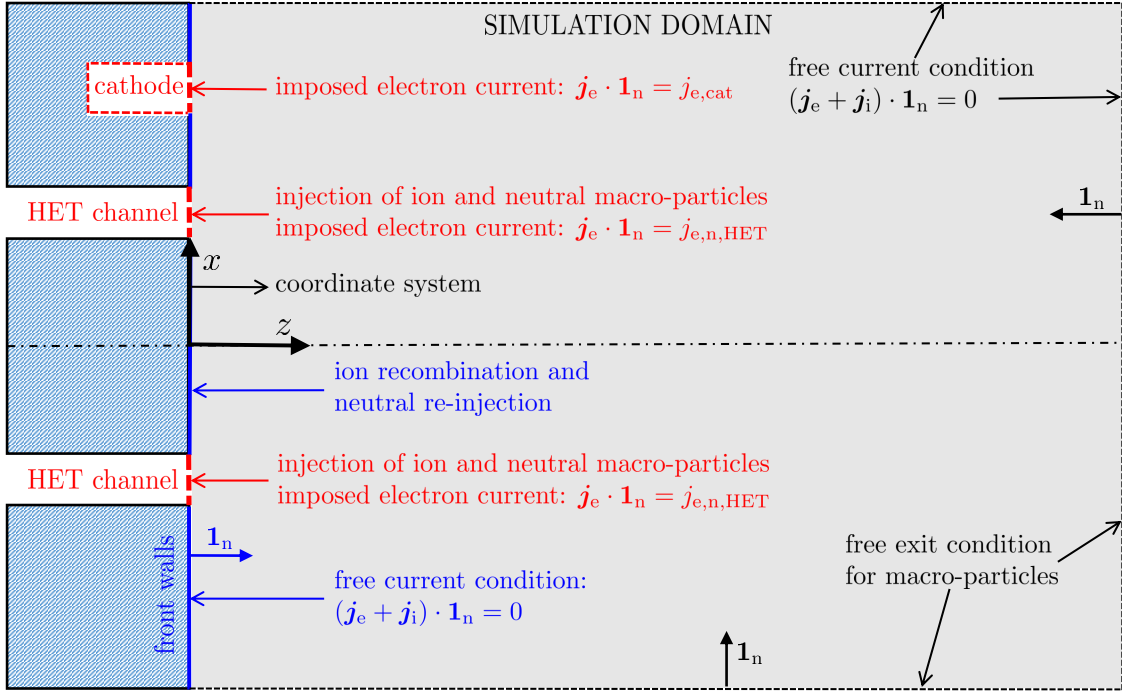


Figure 1. Boundary conditions for both the PIC macro-particles and the fluid electrons, in the considered simulation scenario. The neutralizer is depicted in a lateral position for the sake of clarity, although the nominal case simulation considers a neutralizer at the thruster axis, as reported in Tab. 1.

where Z_s and n_s represent respectively the charge number and the number density of the s^{th} heavy particle population.

With the knowledge of the electron density and of other PIC-related properties, such as the heavy particle fluid velocities and densities \mathbf{u}_s and n_s , the momentum exchange collision frequencies with the heavy species populations ν_{es} , which include both elastic and ionization collisions,¹⁰ the electron model solves the coupled partial differential equations of electron momentum balance and electric current continuity. In particular, for an isotropic electron fluid of negligible inertia, these stationary ($\partial/\partial t = 0$) equations take the form:

$$\begin{cases} 0 = -\nabla p_e - en_e (\mathbf{E} + \mathbf{u}_e \times \mathbf{B}) - \sum_s \nu_{es} m_e n_e (\mathbf{u}_e - \mathbf{u}_s) - \nu_{an} m_e n_e \mathbf{u}_e, \\ 0 = \nabla \cdot (\mathbf{j}_e + \mathbf{j}_i), \end{cases} \quad (3)$$

where $p_e = n_e T_e$ is the electron scalar pressure, m_e is the electron mass, \mathbf{u}_e and \mathbf{u}_s are the fluid velocities of respectively the electrons and the s^{th} heavy particle population, the summation term extends to all heavy particles populations, $\mathbf{j}_e = -en_e \mathbf{u}_e$ and $\mathbf{j}_i = e \sum_s Z_s n_s \mathbf{u}_s$ are respectively the electron and total ion current density, and $\nu_{an} = \alpha_{an} (eB/m_e)$ is an anomalous collision frequency that accounts for the enhanced turbulent transport in HET plasmas.^{4,6} This latter collisional frequency is applied to all directions for the sake of simplicity, as done in most existing hybrid codes.⁶

Under the assumption of barotropic electrons, that is $p_e \equiv p_e(n_e)$, a barotropy state function h_e is introduced, such that $\nabla h_e = \nabla p_e/n_e$ is an exact differential. In this work, a polytropic electron fluid closure is further assumed, so that:

$$h_e(n_e) = -\frac{\gamma T_{e0}}{(\gamma - 1)} \left[1 - \left(\frac{n_e}{n_{e0}} \right)^{\gamma-1} \right], \quad (5)$$

where $\gamma > 1$ is the electron polytropic coefficient and n_{e0} , T_{e0} are the electron density and temperature at a given reference point, where $h_e = 0$.

Let us define $\nu_e = \nu_{an} + \sum_s \nu_{es}$ the total electron momentum transfer collision frequency,

$$\mathbf{j}_c = \frac{en_e}{\nu_e} \sum_s \nu_{es} \mathbf{u}_s \quad (6)$$

an effective current density grouping collisional effects from heavy species (refer to Ref. 10 for the models considered for ν_{es}), and Φ the thermalized potential, such that $\nabla\Phi = \nabla\phi - \nabla h_e/e$. After some straightforward manipulations, the electron momentum equation, Eq. 3, takes the form:

$$0 = en_e \nabla\Phi + \mathbf{j}_e \times \mathbf{B} + \frac{m_e \nu_e}{e} (\mathbf{j}_e + \mathbf{j}_c). \quad (7)$$

If we assume the same reference zero point for Φ , h_e and ϕ , then we have:

$$\Phi = \phi - \frac{h_e}{e} \quad (8)$$

(note that the thermalized potential introduced here is related to the electron Bernoulli energy function $H_e^{10,11}$ by the simple relation $\Phi = -H_e/e$).

In the unmagnetized ($\mathbf{B} = \mathbf{0}$), collisionless ($\nu_e = 0$) limit, this equation yields $\Phi = 0$ and the electric potential satisfies identically the Boltzmann relation $\phi = h_e/e$, as expected. The gradient of the thermalized potential Φ thus measures the correction to that relation due to the magnetic and resistive forces. As pointed out in Ref. 10, most existing plume codes implicitly ignore these corrections, which are absolutely necessary to determine the electron current as shown next. For a finite non-zero total collision frequency ($\nu_e > 0$), solving Eq. 7 for \mathbf{j}_e yields the generalized electron Ohm law

$$\mathbf{j}_e = -\mathcal{K} \cdot (\sigma_e \nabla\Phi + \mathbf{j}_c) \quad (9)$$

where $\sigma_e = e^2 n_e / (m_e \nu_e)$ is the scalar electron conductivity,

$$\mathcal{K} = \begin{bmatrix} 1 & \chi b_z & -\chi b_y \\ -\chi b_z & 1 & \chi b_x \\ \chi b_y & -\chi b_x & 1 \end{bmatrix}^{-1} \quad (10)$$

is the normalized conductivity tensor, $\mathbf{1}_b = (b_x, b_y, b_z)$ is the unit vector along \mathbf{B} , and $\chi = eB/(m_e \nu_e)$ is the effective Hall parameter.

If we substitute Eq. 9 for \mathbf{j}_e into Eq. 4, we finally obtain an elliptic equation for our unknown Φ :

$$\mathcal{K} : \nabla\nabla\Phi + \nabla\Phi \cdot (\nabla \cdot \mathcal{K}) + \mathcal{K} \cdot \nabla\Phi \cdot \nabla \ln \sigma_e = \frac{\nabla \cdot (\mathbf{j}_i - \mathcal{K} \cdot \mathbf{j}_c)}{\sigma_e} \quad (11)$$

where $\nabla\nabla\Phi$ is the Hessian tensor of Φ .

The solution of Eq. 11 requires prescribing the value of Φ or a directional derivative of it at the boundaries of the simulation domain. Referring to Fig. 1, we have assumed a zero net current at all the external boundaries of the simulation domain and at the front walls of the thruster (therefore assumed to be dielectric). At the exit section of the annular channel and of the neutralizer, on the other hand, prescribed normal electron current densities have been imposed. A Dirichlet condition has finally been applied at an inner mesh node).

If $\mathbf{1}_n$ represents the normal direction to the boundary (pointing inwards toward the simulation domain), prescribing a normal current density $j_{e,n} = \mathbf{j}_e \cdot \mathbf{1}_n$ at the boundaries (see Fig. 1), corresponds to imposing the directional derivative of the thermalized potential Φ along the direction $\mathcal{K}^T \cdot \mathbf{1}_n$, which is not necessarily normal to the boundary:

$$\sigma_e (\mathcal{K} \cdot \nabla\Phi) \cdot \mathbf{1}_n = -j_{e,n} - (\mathcal{K} \cdot \mathbf{j}_c) \cdot \mathbf{1}_n, \quad (12)$$

III. Simulations

A. Simulation setup

The plume of an SPT-100 thruster is considered for this analysis,⁴ with the simulation parameters shown in Tab. 1. Three particle populations are considered: the Xe neutrals and both singly and doubly-charged

Table 1. Simulation parameters.

Simulation parameters	Units	Values
Considered PIC populations	-	Xe, Xe ⁺ , Xe ⁺⁺
Total injected ion current	A	3.353
Total thruster mass flow	mg/s	4.296
Total neutralizer mass flow	mg/s	0.215
Singly-charged ions injection velocity	km/s	8.85
Singly-charged ions injection temperature	eV	5.0
Doubly-charged ions injection velocity	km/s	14
Doubly-charged ions injection temperature	eV	9.0
Neutrals injection velocity	km/s	0.45
Neutrals injection temperature	eV	0.07
Front walls temperature	K	500
Neutralizer position (2 cases)	-	($x = y = z = 0$, nominal), ($x = 7.5$ cm, $y = z = 0$)
Reference electron temperature, T_{e0}	eV	35.0
Electron polytropic cooling coefficient, γ	-	1.3
Anomalous diffusion coefficient, α (2 cases)	%	(2.5, nominal), (5.0)
Considered collisions for electrons ¹⁰	-	Elastic and ionizing collisions with Xe ⁺ , Xe ⁺⁺ and Xe
PIC time-step	μ s	0.25
Total simulation time	ms	1.50
Time-averaging steps for PIC sub-model outputs	-	250
Simulation domain physical dimensions	m	0.36 \times 0.36 \times 0.45
Computational grid points	-	121 \times 121 \times 151

Xe ions. The collisions considered for these PIC populations include resonant symmetric CEX collisions between Xe neutrals and both singly and doubly charged ions, single ionization reactions of Xe neutrals and Xe⁺ ions, and double ionization reactions of Xe neutrals.

The total injected ion current into the domain emitted through the annular channel exit area amounts to 3.35 A (1/3 carried by doubly-charged ions), corresponding to a total mass flow of 4.3 mg/s (including neutrals, constituting a 10% of the total mass flow). The neutralizer is modeled as a square emission surface whose center is located at two possible positions (depending on the simulation): $x = y = z = 0$ (emission plane centerline) or at $y = z = 0$ and $x = 0.075$ m (asymmetric position). In both cases, it features 12 mm side and a total injected neutral mass flow of 0.215 mg/s (corresponding to 5% of the thruster mass flow), with no direct ion injection. The injection properties of the heavy particles (fluxes, temperatures and vector fluid velocities) are directly obtained from the simulations of Ref.4 at the exit section of the annular HET channel ($z = 0$). The injection fluxes are shown in Fig. 2 (a), (b) and (c). A singly charged ion flux of approximately $3.5 \cdot 10^{21} \text{ m}^{-2}\text{s}^{-1}$ is injected, versus a flux of doubly charged ions of around $1 \cdot 10^{21} \text{ m}^{-2}\text{s}^{-1}$. The injected neutral flux, on the other hand, is around $6 \cdot 10^{20} \text{ m}^{-2}\text{s}^{-1}$ from the HET channel exit. Regarding the injection velocities, these are predominantly axial (along z) with average values around 14 km/s for doubly-charged ions, 9 km/s for singly-charged ions and 450 m/s for neutrals. The injection temperatures present average values of 5 eV for singly-charged ions, 9 eV for doubly-charged ions, and 0.09 eV for neutrals. Finally, the neutralizer neutrals are injected with a uniform flux of $6.8 \cdot 10^{21} \text{ m}^{-2}\text{s}^{-1}$, a sonic fluid velocity of 300 m/s and a temperature of 0.07 eV.

In order to model the interaction of ions and neutrals with the front walls of the thruster, these are assumed to be at a uniform temperature of 500 K. As mentioned in Sec. IIA, both recombined ions and reflected neutrals are emitted diffusely, assuming a perfect thermal equilibrium with the walls.

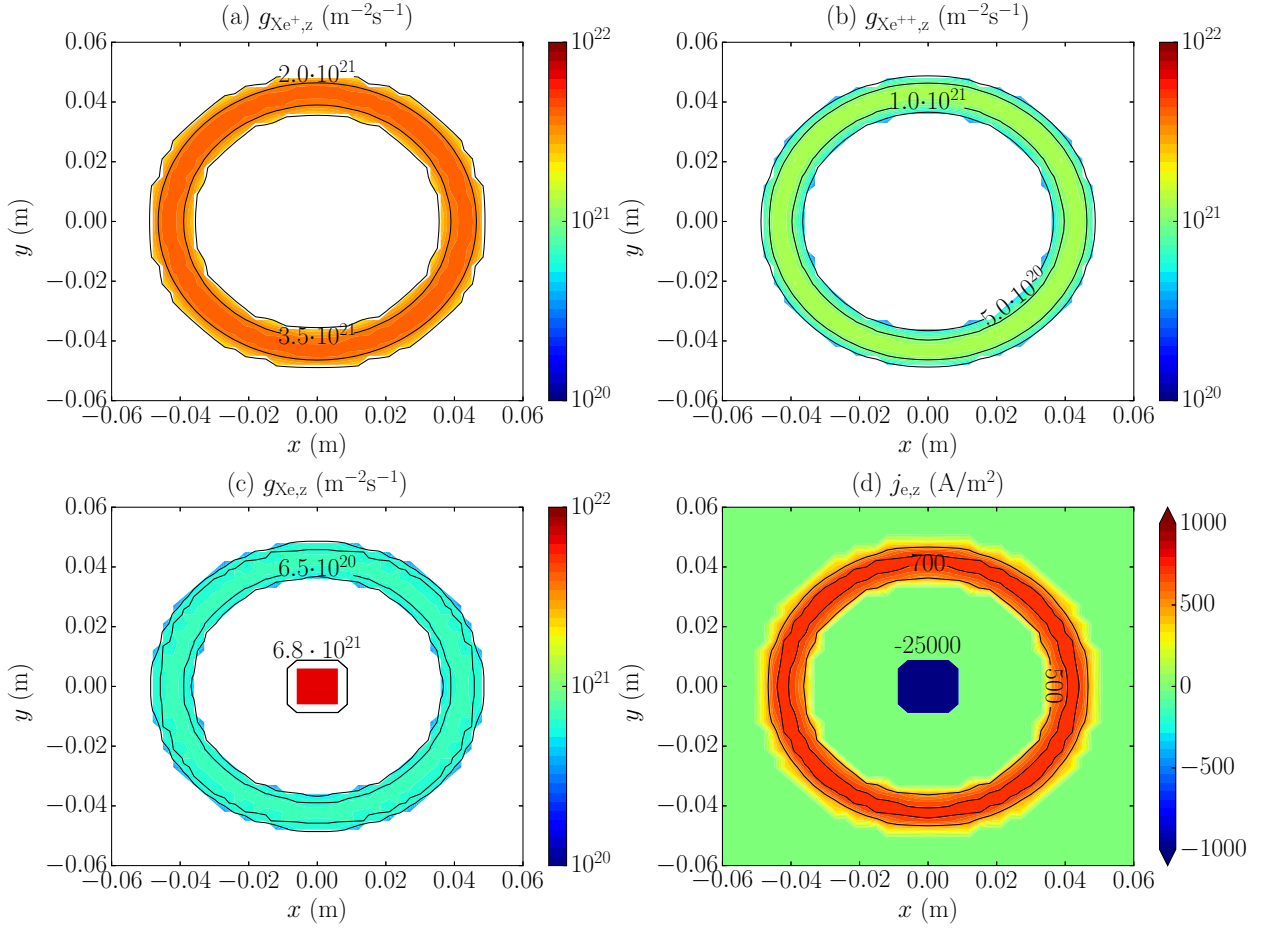


Figure 2. Imposed injection fluxes at $z = 0$ for (a) singly-charged ions, (b) doubly-charged ions, (c) neutrals, and (d) normal electron current density at $z = 0$. For these plots, a centerline neutralizer is considered. The side of the neutralizer emission area is 1.2 cm, equivalent to 4 PIC cells.

Regarding the electron fluid, this presents a prescribed normal flux $j_{e,n}$ at $z = 0$ as shown in Fig. 2 (d), featuring a symmetric cathode at the thruster axis. While the electron flux at the channel exit has been obtained from the 2D simulation results,⁴ the flux emitted by the surface cathode is such that the total electron current towards the boundaries equals, in magnitude, the total ion current. As already mentioned in Sec. II B, electrons are assumed to be polytropic with a coefficient $\gamma = 1.3$, typical of several experimental characterizations of HET plumes,⁸ and a reference temperature of 35 eV at a point just downstream from the exit channel mid-point. Electron collisions include both elastic and inelastic (ionization) collisions with singly and doubly-charged ions and with neutrals. Moreover, in order to account for the anomalous transport, an anomalous diffusion coefficient $\alpha_{an} = 2.5\%$ has been considered for the nominal case.

The PIC time step is 0.25 μs , while the simulation duration is 1.5 ms, sufficiently long to reach stationary conditions in the results. The simulation domain is 0.36 m wide in both x and y , while 0.45 m along z , with a total number of nodes equal to $121 \times 121 \times 151$. This corresponds to a uniform Cartesian mesh with cubic cells of 3 mm side. The total number of macro-particles at stationary conditions is around $45 \cdot 10^6$.

Finally, a total of three simulation cases have been considered in this work:

- A nominal simulation with a neutralizer at the thruster axis and $\alpha_{an} = 2.5\%$.
- A simulation with a neutralizer at the thruster axis and $\alpha_{an} = 5.0\%$.
- An asymmetric simulation with a neutralizer on one side of the thruster and $\alpha_{an} = 2.5\%$.

B. Nominal simulation results

The magnetic field magnitude and streamlines are shown in Fig. 3 (a). The peak magnetic field is found at the injection plane centerline and is close to 200 Gauss. At $z > 25$ cm the magnetic field has already dropped to less than 1 Gauss and presents values close to 0.1 Gauss at the downstream section ($z = 45$ cm). The considered magnetic circuit features a null point at $z = 10$ cm at the thruster centerline. The corresponding map of the Hall parameter χ is shown in Fig. 3 (b). The Hall parameter is dominated everywhere by the anomalous collision frequency ν_{an} so that it tends to the limiting value (for negligible collisionality with the heavy species) of $1/\alpha_{an} = 40$ almost everywhere, with the exception of the magnetic field null-point, where it reaches values around 10.

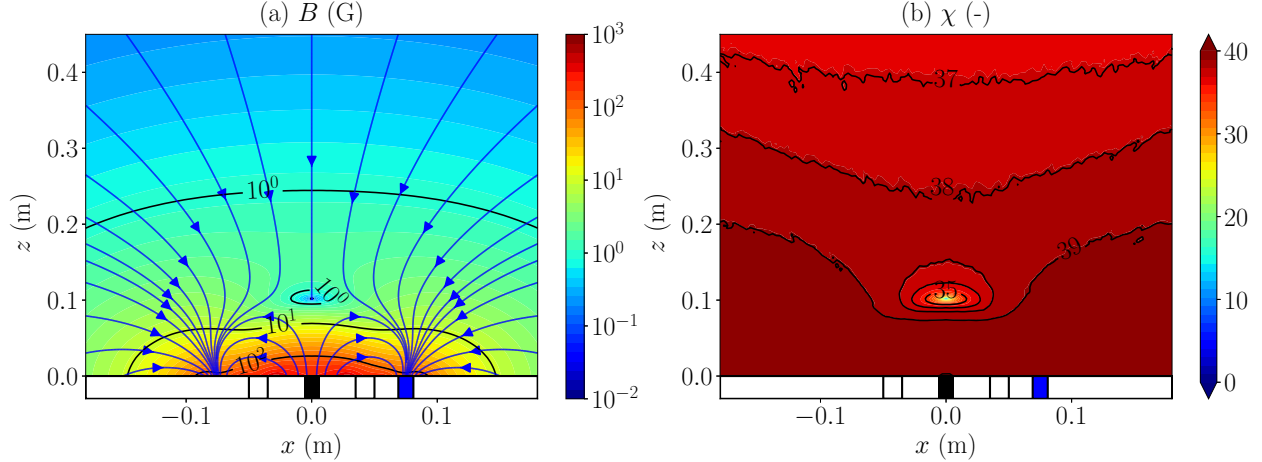


Figure 3. Nominal simulation results at $y = 0$ showing: (a) magnetic field magnitude and streamlines, and (b) Hall parameter. The projection of the thruster and annular channel walls with the $x - z$ plane are shown by the black solid lines at $z < 0$, while the neutralizer is indicated by either a black (symmetric cases) or blue (asymmetric case) rectangle.

The nominal simulation results at the meridional plane ($y = 0$) are shown in Fig. 4 (a) to (f). The electron density (Fig. 4 (a)) becomes single-peaked at less than 10 cm downstream from the HET channel exit. Two separate peaks of almost 10^{18} m^{-3} can be appreciated at the channel exits and at the thruster centerline ($x = 0$), where the neutralizer is located. The plasma density drops to less than 10^{16} m^{-3} at a distance of 30 cm downstream. The corresponding electron temperature is shown in Fig. 4 (b) and presents peak values close to 35 eV at the channel exits (where the reference point for the electron fluid is located) and close to the centerline neutralizer. The electron temperature drops to almost 7-8 eV at the downstream section. The singly-charged ion density is shown in Fig. 4 (c) and looks quite similar to the electron density with minor differences due to the presence of doubly-charged ions. These present a density that is approximately one order of magnitude lower than that of the singly-charged ions. Fig. 4 (d) then shows the neutral density, featuring a peak at the neutralizer and at the HET channel exits. This peak at the neutralizer is responsible of a large local ionization rate and hence a large electron density at the neutralizer. This yields a peak of the barotropy function (refer to Eq. 5), as commented in the following paragraph.

The electric potential is shown in Fig. 4 (e). In these plots, all potentials have been assumed to be 0 at the neutralizer exit. Ions suffer a total potential drop of around 150 V (from the HET exit channel). The difference of potential with the centerline cathode is only around 10 V, due to the local electron density peak at the neutralizer. The thermalized potential Φ is shown in Fig. 4 (f). As expected, its gradient is important close to the exit section of the thruster (for $z < 5$ cm) where it is clearly dominant over the barotropy function gradient and produces equi-potential lines that are almost parallel to the local magnetic field.

The electron in-plane current density and the corresponding electron fluid velocity vector direction are shown in Fig. 4 (g). Since electrons are strongly magnetized, they cannot easily traverse the magnetic field lines, so they generally travel parallel to them (or in the azimuthal out-of-plane direction). The neutralizer electrons (emitted at the centerline) flow either towards the HET channel (constituting the anode electron current) or downstream to neutralize the ion current. The out-of-plane current density $j_{e,y}$ (i.e. azimuthal) is finally shown in Fig. 4 (h). As expected, such a Hall current density produces a positive downstream

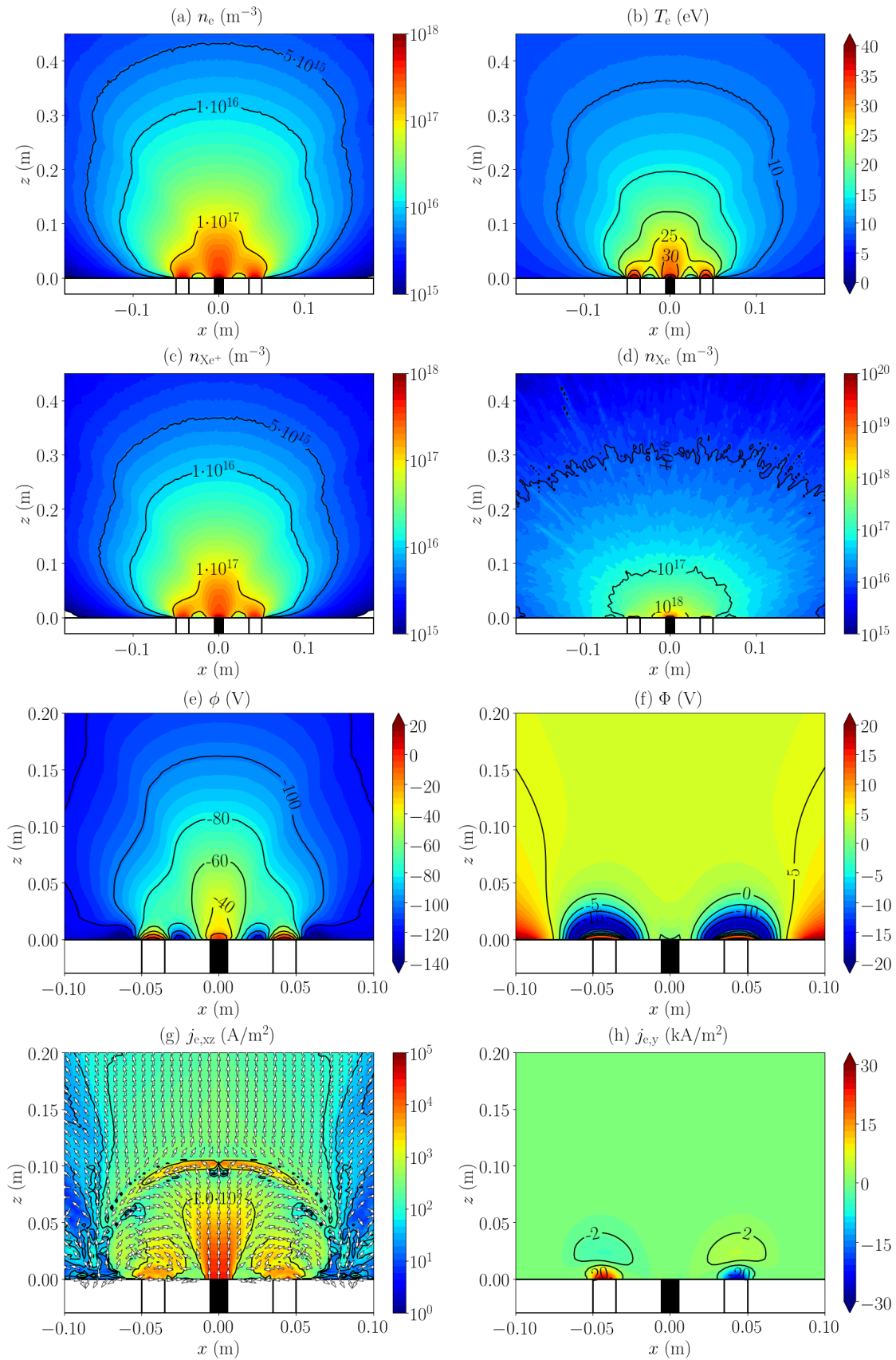


Figure 4. Nominal simulation results at $y = 0$ showing: (a) electron density, (b) electron temperature, (c) singly-charged ion density, (d) neutral density, (e) electric potential, (f) thermalized potential, (g) electron current density and fluid velocity vector direction in the plane, and (h) out-of-plane electron current density. The projection of the thruster and annular channel walls with the $x - z$ plane are shown by the black solid lines at $z < 0$, while the neutralizer is indicated by the black rectangle.

acceleration of the plasma ($(\mathbf{j}_e \times \mathbf{B})_z = -j_y B_x > 0$), and hence a positive magnetic thrust, consistently with the results of Ref. 4 and the physics of HETs. Moreover, as theoretically expected, the peak azimuthal current density is located at the HET channel exit and is approximately $\chi = 40$ times larger than the imposed axial electron current density there (30000 A/m^2 vs 700 A/m^2 , refer to Fig. 2 (d) for this latter axial electron current density).

Finally, Fig. 5 (a) and (b) show respectively at the $z = 0$ emission plane, the total ion flux (due to both singly and doubly-charged ions) and the corresponding ion wall average impact energy (per elementary particle). The latter has been computed taking into account also the electric potential drop occurring in the dielectric plasma sheath located at the front thruster walls. Both the flux and the impact energies are maximum between the neutralizer and the HET channel, with values of respectively $10^{20} \text{ m}^{-2}\text{s}^{-1}$ and 200 eV . At radii larger than the outer HET channel radius, the ion flux reduces to between 10^{18} and $10^{19} \text{ m}^{-2}\text{s}^{-1}$, and the average impact energy to less than 150 eV . The non-circular pattern that can be observed in the iso-lines of both flux and impact energy is due to the rectangular shape of the neutralizer which slightly affects the electric potential distribution, at the $z = 0$ cross section, and strongly influences the trajectories of slow-ions produced by CEX and ionization. Such geometrical effect can be mitigated by assuming a circular emission cathode, however, this has not been implemented in this work, given the low number of available cells to characterize the neutralizer emission area (4×4).

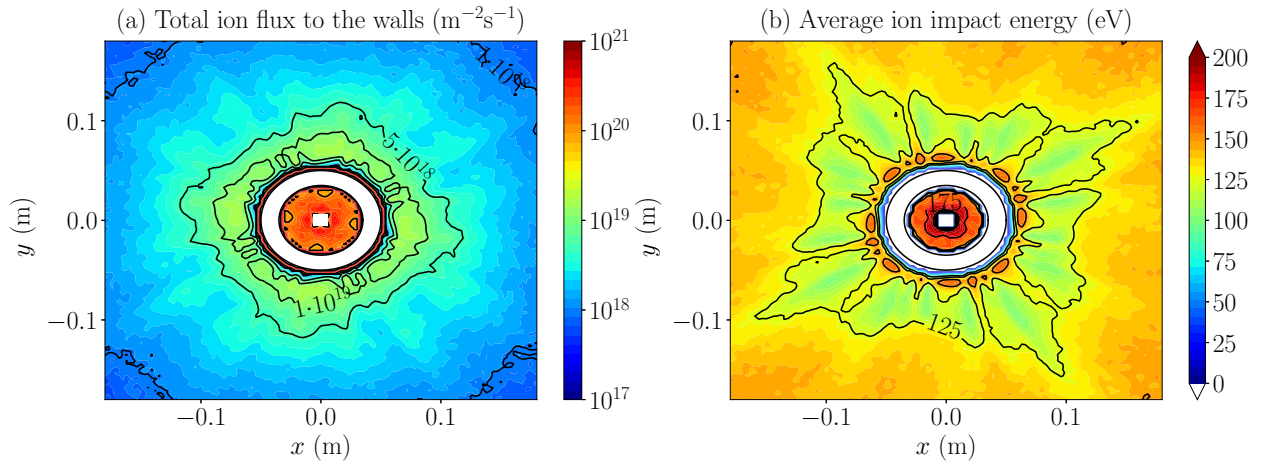


Figure 5. (a) Ion flux and (b) mean impact energy on the front walls of the HET.

C. Effects of the anomalous diffusion coefficient

A similar simulation has been carried out with the same injection conditions described in Sec. III A but with a larger anomalous diffusion coefficient. Now we have set it to 5% (versus the 2.5% considered for the nominal case). The two simulations are compared in Figs. 6 and 7.

The electron density (and hence the heavy species density) does not suffer any significant variation with respect to the nominal case, as shown in Fig. 6 (a) (refer to the red dashed and black solid lines). The nominal case density is just a few percent higher at the downstream section, due to a slightly more focused beam (due to a larger acceleration close to the HET channel exit). The same occurs for the electron temperature, with the nominal case showing slightly higher values.

In the increased anomalous transport case, the difference between the electric potential at the HET channel exit and at the neutralizer surface reduces from around 10 V (see Fig. 4 (e)) to only 5 V . Along the HET channel centerline (i.e. along the axial line located at the mid-radius of the HET channel), ions see a slightly higher potential drop (5 V higher) in the nominal case, as shown in Fig. 7 (a) (refer again to the red dashed and black solid lines). This higher ion acceleration produces a more focused ion beam and hence slightly higher densities downstream, as seen in Fig. 6 (a). Regarding the out-of-plane current density along the HET channel centerline, shown in Fig. 7 (b), the nominal case features values that are exactly twice those of the $\alpha_{\text{an}} = 0.05$ case, close to the HET channel exit section ($z = 0$). This is indeed due to the fact that the axial electron current is fixed in both cases, while the Hall parameter is around 40 in the nominal

case, versus 20 in this increased anomalous transport case.

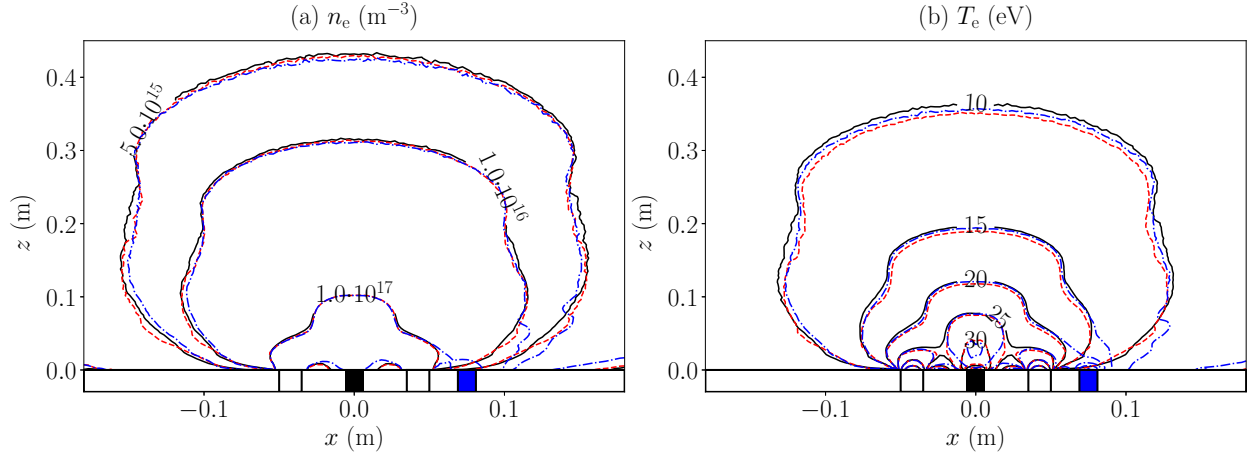


Figure 6. Comparison of nominal simulation ($\alpha = 0.025$, black solid lines), higher anomalous transport simulation ($\alpha = 0.05$, red dashed lines) and lateral neutralizer simulation ($\alpha = 0.025$, blue dash-dot lines) at $y = 0$ showing: (a) electron density, and (b) electron temperature. The projection of the thruster and annular channel walls with the $x - z$ plane are shown by the black solid lines at $z < 0$, while the neutralizer is indicated by either a black (symmetric cases) or blue (asymmetric case) rectangle.

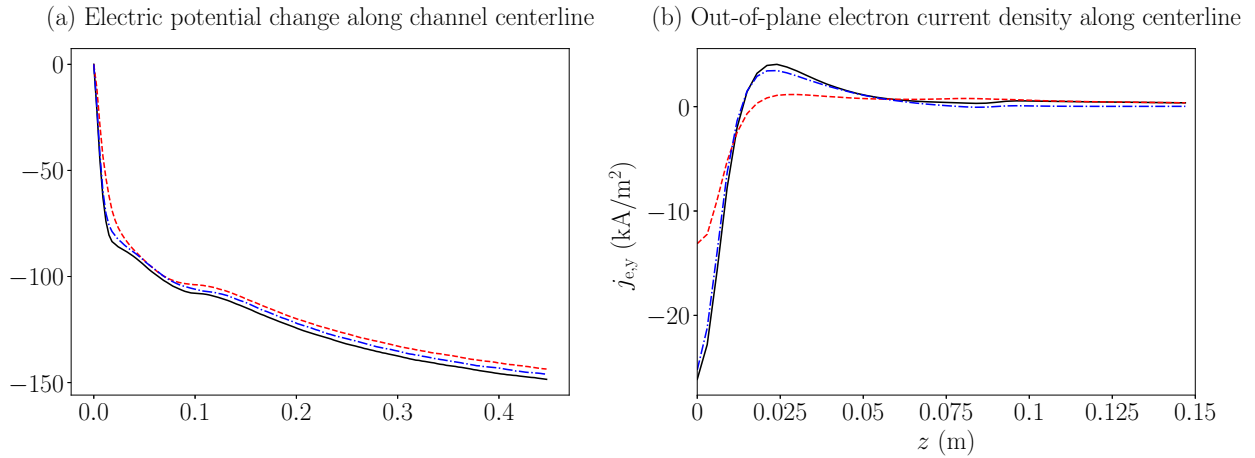


Figure 7. Comparison of nominal simulation ($\alpha = 0.025$, black solid lines), higher anomalous transport simulation ($\alpha = 0.05$, red dashed lines) and lateral neutralizer simulation ($\alpha = 0.025$, blue dash-dot lines) showing the 1D evolutions of: (a) electric potential change, and (b) aximuthal electron current density along the HET channel centerline.

These results show that the anomalous transport coefficient in the near-plume does not affect greatly the heavy species densities and velocities, so that thruster performance figures such as specific impulse and thrust can be reasonably estimated by using a rough value of the anomalous diffusion coefficient. Nevertheless, we point out that the use of a different anomalous diffusion coefficient inside the discharge chamber, as modeled by the source 2D code,⁴ might produce very different heavy particles injection profiles at $z = 0$, hence producing bigger changes in such thruster performance figures.

D. Effects of an asymmetric neutralizer position

The last simulation case considered features a lateral neutralizer, whose exit surface center is now located at $x = 0.075$ m and $y = z = 0$ and features the same size and shape as in the previous simulations (square with 12 mm side, e.g. 4 cells). Such simulation is clearly asymmetric and cannot be carried out with axisymmetric 2D codes. It is therefore of interest to assess to what extent the neutralizer position affects the near-plume

physics. The results are presented in Fig. 8 and are discussed below.

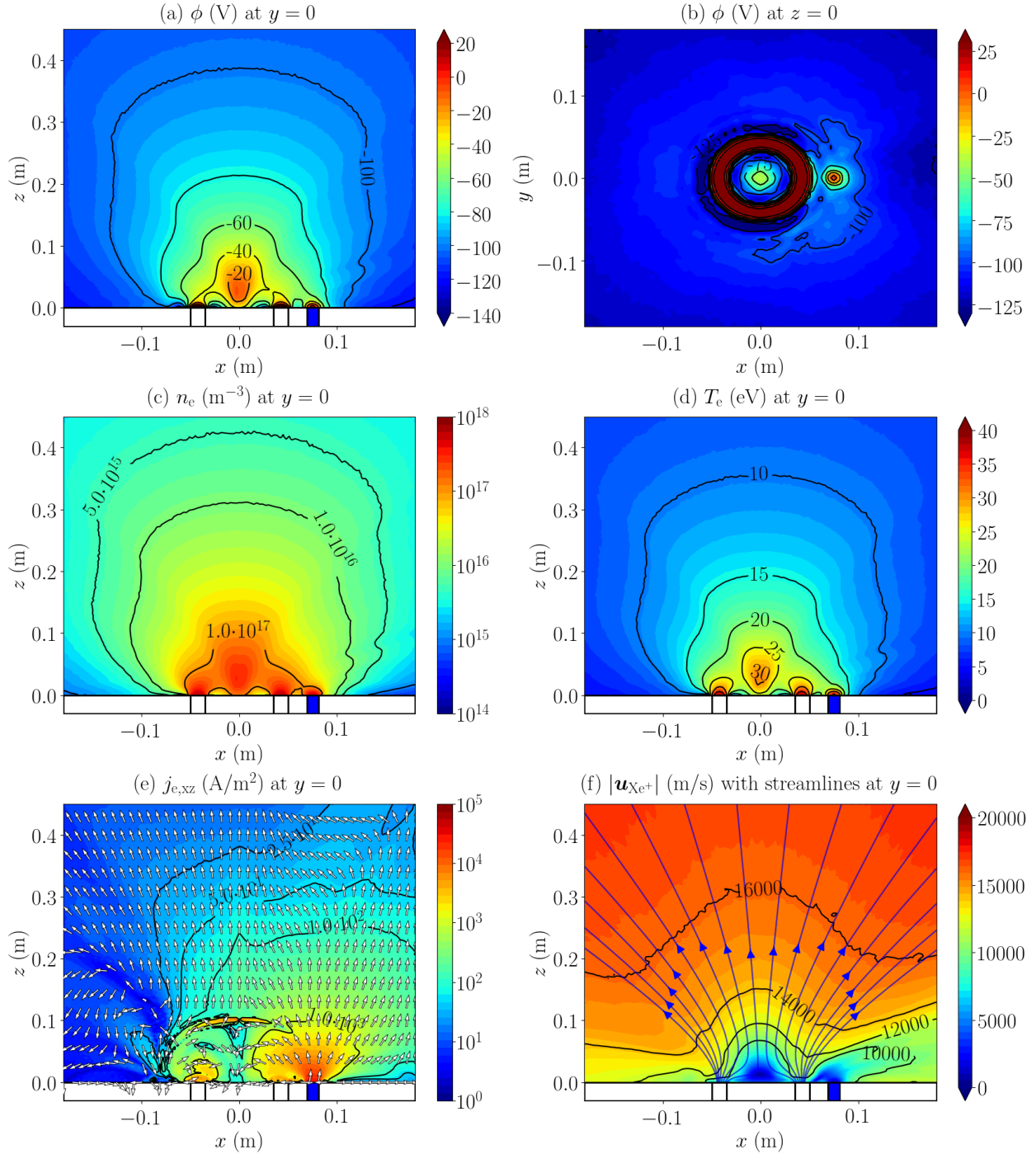


Figure 8. Results of the lateral neutralizer case ($\alpha_{an} = 0.025$): (a) electric potential at $y = 0$, (b) electric potential at $z = 0$, (c) electron number density at $y = 0$, (d) electron temperature at $y = 0$, (e) in-plane electron current density and fluid velocity vector direction, and (f) singly-charged ion fluid velocity and streamlines. The ion exit velocity from the annular channel is around 9 km/s. The projection of the thruster and annular channel walls with the $x-z$ plane are shown by the black solid lines at $z = 0$, while the neutralizer is indicated by the blue rectangle.

Fig. 8 (a) shows the electric potential distribution at $y = 0$. The lateral cathode perturbs the electric potential locally, as shown in Fig. 8 (b) at the injection plane cross section $z = 0$. Nevertheless, this asymmetry disappears quickly downstream.

Fig. 8 (c) shows the electron number density at $y = 0$. The asymmetry introduced by the neutralizer quickly disappears and the results are almost symmetric at a distance of only 10 cm downstream from the exit surface of the HET. The same can be observed in Fig. 8 (d), showing the electron temperature at $y = 0$.

Fig. 8 (e) shows the electron current density at $y = 0$ with the electron fluid velocity direction. Now, electrons are emitted from a lateral position and, once again, they either neutralize downstream the ion beam, or they go inwards and constitute the anode electron current. A large asymmetry is produced by the presence of the lateral cathode and persists even at more downstream sections.

Fig. 8 (f) shows the singly-charged ions fluid velocity and streamlines. Ions reach downstream velocities beyond 16 km/s, close to the expectations for this type of thruster (operating with a total discharge voltage of 300 V). In this case, the asymmetry induced by the neutralizer disappears almost completely downstream.

Finally, as clearly shown in Figs. 6 and 7 (refer to the dash-dot blue and solid black lines), it can be appreciated that the variations (with respect to the nominal case) of electron density, temperature, azimuthal electron current density and electric potential are small.

In summary, the neutralizer lateral position does not introduce significant asymmetries in the electric potential and heavy particle properties, such as the ion current and number densities, or the electron number density and temperature (which both depend on the heavy particles density). Nevertheless, the asymmetry persists in the electron current density and streamlines, which are strongly affected by the neutralizer position.

E. Comparison with HYPHEN 2D code results

The results of the asymmetric neutralizer case are here compared with those of the 2D HYPHEN code, which, as mentioned in the introduction, determines the electron temperature consistently by solving the electron energy balance equation.

A first important point is that the assumption of an asymmetric cathode produces also an asymmetric electron current distribution, contrary to the symmetric results obtained in the 2D simulation, which implicitly assumes an axi-symmetric ring-like neutralizer. In fact, Fig. 8 (e) clearly shows this asymmetry in the electron current density distribution. Nevertheless, especially in the very near-plume ($z < 10$ cm), electrons appear to distribute almost uniformly along the magnetic field lines, and through the strong azimuthal drift, they also reach the other side of the HET channel (with respect to the neutralizer position). Moreover, the position of the neutralizer does not affect significantly the heavy species particle properties, thus justifying the use of an axisymmetric code, at least for the accurate estimation of the thruster performance figures.

Secondly, a comparison of the results obtained with the two codes permits to cross-verify the 2 codes, by observing that, just downstream of the HET channel exit section, the predicted electric fields are very similar. This can be appreciated in Fig. 9 (a) and (b), showing respectively the electric potential distribution of the 3D and 2D code. It is underlined that this similarity is achieved through the computation of the thermalized potential Φ , whose gradient at the exit section (40 V in 1 cm, see Fig. 4 (f)) is dominant compared to the electron barotropy function gradient. For this reason, the iso-potential lines turn out to be almost parallel to the magnetic field, as in the 2D simulation.

However, Fig. 9 (c) and (d) show that the polytropic assumption to compute the electron temperature is clearly far from the more detailed energy model of the 2D code. In fact, while the electron temperature decreases mildly in the 3D simulation, as it strictly follows the plasma density evolution as $T_e = T_{e0} (n_e/n_{e0})^{\gamma-1}$, the 2D code predicts a much quicker decay: the electron temperature descends from around 30-35 eV at $z = 1$ cm (along the channel centerline) to only 9 eV at $z = 3$ cm. As also shown in Ref. 4, the electron temperature does not follow the plasma density but it rather presents iso-contour lines that are almost parallel to the magnetic field lines (a fact that cannot be reproduced by the 3D model based on polytropic electrons).

Clearly, these large differences in the prediction of the electron temperature affect strongly the electric potential distribution. While the electric fields are quite similar in the first cm of the expansion, the predicted maps quickly diverge from one another downstream. While in the 3D simulation, the electric potential map gradually follows that of the electron barotropy function h_e (see Eq. 5), in the 2D simulation, the electron pressure drop is much stronger and induces a larger drop in electric potential, which reaches a negative peak around -190 V at $z \simeq 3$ cm. This highlights the importance of accurate electron models in the simulation of HETs. Moreover, apart from the different approach to compute the electron temperature, there are two additional differences in the considered models with a non-negligible effect: (*i*) the 2D simulation cathode is being modeled as a volumetric cathode source located inside the plasma plume domain (versus a surface cathode at the upstream boundary of the 3D simulation), and with no neutral mass flow injection, so that no

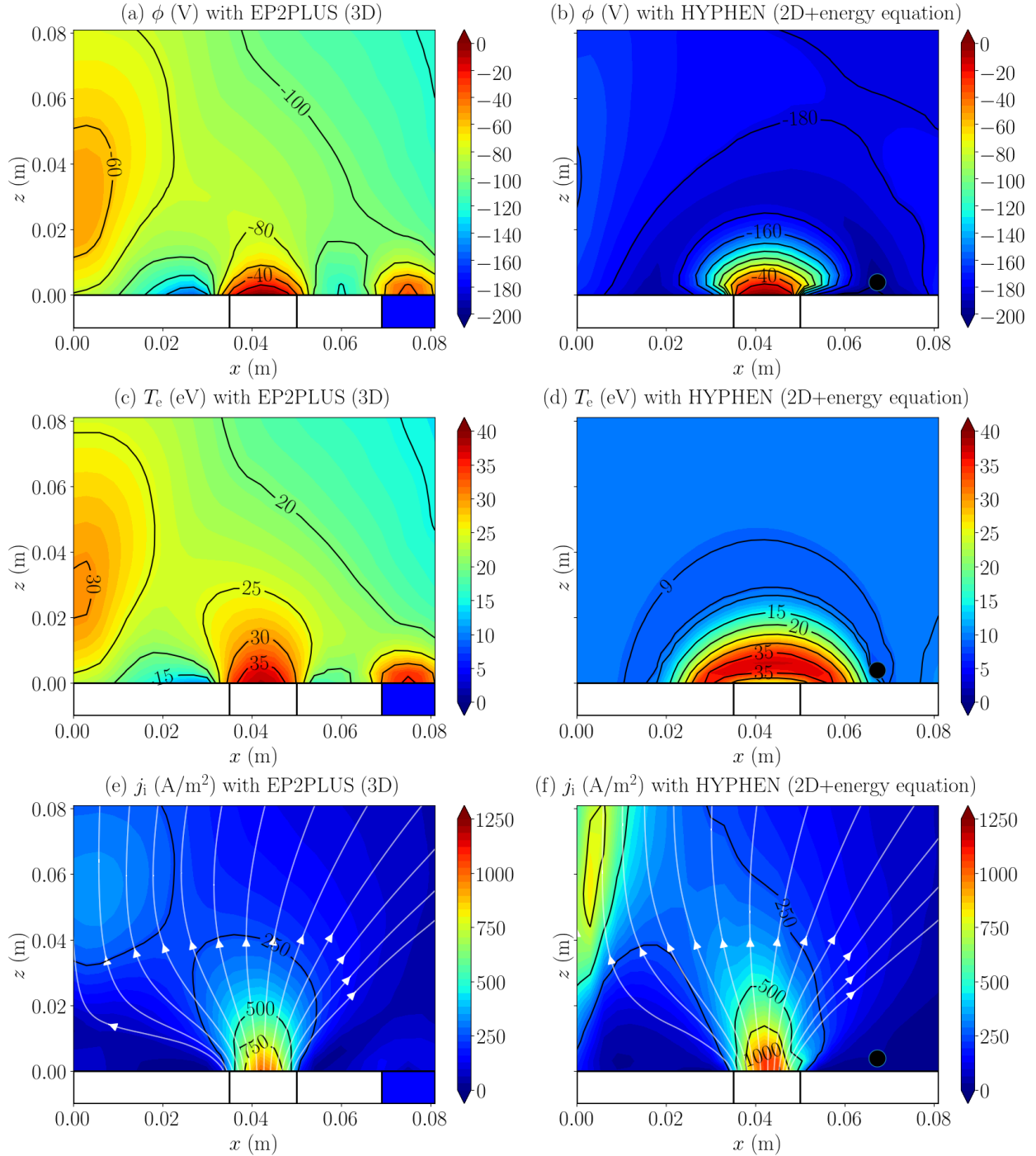


Figure 9. Comparison between the EP2PLUS asymmetric cathode simulation (a,c,e) and the 2D HYPHEN simulation (b,d,f) of: electric potential (a,b), electron temperature (c,d) and ion current density with streamlines (e,f), at $y = 0$. The electric potential is re-scaled to be 0 at the HET channel exit plane. The projection of the thruster and annular channel walls with the $x-z$ plane are shown by the black solid lines at $z < 0$, while the neutralizer is indicated by the blue rectangle in subplots (a), (c) and (e) and by a black circle in subplots (b), (d) and (f) (HYPHEN considers a volumetric cathode source).

plasma density peak is observed there, and (ii) the 2D cathode electric potential is being directly imposed as a boundary condition (while in 3D simulations we can only act on the thermalized potential, and more precisely on its gradient). All these effects contribute to create the differences that can be observed in Fig. 9

(a) and (b).

The total ion current density is finally shown in Fig. 9 (e) and (f). The general shape of the ion streamlines and the current density values appear to be quite similar in both simulations, although this is, in part, due to the fact that the 3D code considers the results of the 2D simulation at the HET exit plane as boundary conditions for the injection of the heavy particles.

IV. Conclusions

In this paper, a 3D hybrid PIC code, named EP2PLUS, has been used to simulate a Hall effect thruster near-plume expansion, considering the effects of the magnetic field and of the anomalous turbulent diffusion in the fluid electron momentum equation.

The most innovative part of the hybrid model is represented by the magnetized electron fluid model, which features a formulation in terms of a thermalized potential, and assumes polytropic electrons. This simplification is generally a good one sufficiently far away from the thruster exit plane, and here, we have investigated the consequences of doing so in the near-plume, by comparing the results obtained with EP2PLUS with those of a 2D companion code, HYPHEN (see Ref.4) that solves the electron energy balance equation in a magnetically aligned mesh.

Simulations with two different anomalous transport coefficient (2.5 and 5%) have shown that the effects of this tunable parameter on the near-plume expansion physics are not so important, except for the estimation of azimuthal currents, as far as the correct order of magnitude is assumed (a few percent).

EP2PLUS has been further used to simulate a clearly 3D scenario featuring an asymmetric position of the neutralizer, now considered to be at one side of the exit channel. This simulation has shown that relevant changes with respect to the axisymmetric case are found only in the electron streamlines and current density. Other properties, such as the electric potential or the ion current density remain essentially axisymmetric, a fact that justifies the use of axisymmetric 2D codes for Hall effect thruster performance estimation.

Finally, EP2PLUS and HYPHEN simulations have been compared to assess the consequences of neglecting the electron energy equation in the former. In the 3D EP2PLUS simulation, the electric iso-potential lines are parallel to the magnetic field lines only very close to the HET channel exit. In this small region, where the magnetic field dominates and the electron temperatures are similar, EP2PLUS and HYPHEN provide very similar electric fields. However, already a few cm downstream, the electric potentials start to diverge significantly, which can be explained by several differences in the models. First of all, the assumption of polytropic electrons in EP2PLUS, is not capable of reproducing the expected iso-thermality of magnetic field lines and the large drop in electron pressure predicted by HYPHEN (in the 3D simulation, on the other hand, the electron temperature and hence the pressure decay much more slowly). Secondly, HYPHEN simulations consider a volumetric cathode source (versus the surface cathode of EP2PLUS) and do not include the injection of neutrals, which can be ionized and affect importantly the electric potential distribution. Finally, contrary to the 3D model, the 2D model can directly impose the cathode electric potential, so that the electric potential is forced to descend to the cathode value when the cathode magnetic field line is reached.

Acknowledgments

This work has been supported by the CHEOPS project, funded by the European Union's Horizon 2020 Research and Innovation Programme (Grant 730135). Additional funding for F. Cichocki came from Project ESP2016-75887 (Spain's National Research and Development Plan - MINECO/ FEDER).

References

¹Tajmar, M., Gonzalez, J., and Hilgers, A., "Modelling of spacecraft-environment interactions on SMART-1," *Journal of Spacecraft and Rockets*, Vol. 38, No. 3.

²Tajmar, M., Meissl, W., González, J., Foing, B., Laakso, H., Noci, C., Capacci, M., Mälkki, W., and Darnon, F., "Charge-exchange plasma contamination on SMART-1: First measurements and model verification," *40th Joint Propulsion Conference and Exhibit*, paper 2004-3437, American Institute of Aeronautics and Astronautics, Reston, VA, Fort Lauderdale, Florida, July 11-14, 2004.

³Pérez-Grande, D., *Fluid modeling and simulation of the electron population in Hall effect thrusters with complex magnetic topologies*, Ph.D. thesis, Universidad Carlos III de Madrid, Leganés, Spain, 2018.

⁴Domínguez-Vázquez, A., Fajardo, P., and Ahedo, E., "Analysis of the plasma discharge in a Hall thruster via a hybrid

2D code,” 36th *International Electric Propulsion Conference*, No. IEPC-2019-579, Electric Rocket Propulsion Society, Vienna, Austria, 2019.

⁵Ortega, A. L., Mikellides, I. G., and Chaplin, V. H., “Numerical Simulations for the Assessment of Erosion in the 12.5-kW Hall Effect Rocket with Magnetic Shielding (HERMeS),” *35th International Electric Propulsion Conference, Atlanta, GA, IEPC-2017-154*, 2017.

⁶Taccogna, F. and Garrigues, L., “Latest progress in Hall thrusters plasma modelling,” *Reviews of Modern Plasma Physics*, Vol. 3, No. 1, 2019, pp. 12.

⁷Beal, B., Gallimore, A., and Hargus, W., “Preliminary plume characterization of a low-power Hall thruster cluster,” *Proc. 38th Joint Propulsion Conference, Indianapolis, IN*, AIAA-2002-4251, 2002.

⁸Beal, B., Gallimore, A., and Hargus, W., “Plasma properties downstream of a low-power Hall thruster,” *Physics of Plasmas*, Vol. 12, No. 12, 2005, pp. 123503.

⁹Cichocki, F., Domínguez, A., Merino, M., and Ahedo, E., “A 3D hybrid code to study electric thruster plumes,” *Space Propulsion Conference 2016*, No. paper 2016-3124968, Association Aéronautique et Astronautique de France, Rome, Italy, May 2-6, 2016.

¹⁰Cichocki, F., Domínguez-Vázquez, A., Merino, M., and Ahedo, E., “Hybrid 3D model for the interaction of plasma thruster plumes with nearby objects,” *Plasma Sources Science and Technology*, Vol. 26, No. 12, 2017, pp. 125008.

¹¹Cichocki, F., Merino, M., and Ahedo, E., “A 3D electron fluid model to study magnetic field effects on an expanding plasma thruster plume,” *Space Propulsion Conference 2018*, No. 00295, Association Aéronautique et Astronautique de France, Seville, Spain, May 14-18, 2018.

¹²Hockney, R. and Eastwood, J., *Computer simulation using particles*, CRC Press, Boca Ratón, FL, 1988.